Experimental investigation of the dynamic behaviour of a fully passive flapping foil hydrokinetic turbine

Leandro de Carvalho Duarte, Nicolas Dellinger, Guilhem Dellinger, Abdallah Ghenaim, Abdelali Terfous

Experimental investigation of the dynamic behaviour of a fully passive flapping foil hydrokinetic turbine †

†Postprint 2019, Journal of Fluids and Structures
Published version available at https://doi.org/10.1016/j.jfluidstructs.2019.04.012

L. Duarte[a,*], N. Dellinger[a], G. Dellinger[a,b], A. Ghenaim[a,c], A. Terfous[a,c]

[a] *ICube laboratory, Département mécanique, Université de Strasbourg, France*
[b] *École Nationale du Génie de l'Eau et de l'Environnement de Strasbourg, France*
[c] *Institut National des Sciences Appliquées de Strasbourg, France*

Abstract

The dynamic behaviour of a fully passive flapping foil hydrokinetic turbine is experimentally investigated at a Reynolds number of 6×10^4. Previous numerical simulations showed that, depending on the location of the pitching axis l_θ and the rotational stiffness k_θ, four different responses may emerge from the system. Only one of them is suitable for energy harvesting purposes, which is characterised by large amplitude pitching and heaving oscillations about the equilibrium position. The present work experimentally validates these findings. A nondimensionalised chart delimiting the boundaries between the different responses in the parameter space $l_\theta \times k_\theta$ is provided, relying upon an original quantitative classifying map. It has been found that the pitching axis must be placed at least 29% of the chord length behind the leading edge in order for the foil to present a non stationary response. The ideal behaviour for harvesting purposes can be achieved without any pitching stiffness for a pitching axis location from 31% to 39% of the chord length, some pitching stiffness being needed for values above that range. Finally, sensitivity tests revealed a slight dependence of the transition boundaries on the heaving mass m_y and stiffness k_y, suggesting that an increase in the heaving natural frequency of the baseline prototype may help the system respond in the desired way for an energy extraction scenario.

Keywords: flapping foil, hydrokinetic turbine, stability analysis, fluid-structure interaction, renewable energy.

1. Introduction

In a time of a rapidly growing global demand for clean and renewable energy, significant effort has been made in order to develop alternative decentralised energy generation solutions. Besides meeting this need, the development of innovative micro-hydro power plants shows to be a promising way to supply electricity to rural and isolated areas. The flapping foil hydrokinetic turbine is one of these novel concepts that has attracted considerable attention from the scientific community over the past decades (see review papers by Xiao and Zhu (2014) and Young et al. (2014)).

Bio-inspired from aquatic animals, a flapping foil hydrokinetic turbine consists of a blade performing oscillatory rotation (pitching) and translation (heaving) motions in perpendicular directions to the flow. With an appropriate synchronism between the heaving velocity and fluid forces over the foil, the system is capable of harvesting the kinetic energy of the flow. This can be achieved by prescribing the two motions through coupling mechanisms or external actuators. For such constrained flapping foil designs, Davids (1999) and Kinsey and Dumas (2008) found that the pitching axis location is a key parameter in ensuring the desired synchronism and the appropriate phase lag between heaving and pitching motions. Later, Kinsey et al. (2011) designed and tested a constrained flapping foil prototype, reporting a hydraulic efficiency of 40% (ratio between the power harvested and the power available in the flow). In spite of the high energy extraction performances, the complexity related to the coupling mechanisms encouraged the research for alternative designs.

A much simpler and challenging idea, originally proposed by Peng and Zhu (2009), is to elastically mount the foil and leave the heaving and pitching motions to be completely induced by the fluid-structure interactions. In this fully passive design, the synchronism between the foil motions and the flow dynamics to enable the energy extraction regime must be achieved through a fine-tuning of all its structural parameters. Depending on the pitching axis location and the pitching stiffness, numerical simulations performed by Peng and Zhu (2009) suggested the existence of four different responses. Following Peng and Zhu (2009) and Zhu (2012), the desired response for energy harvesting purposes can be achieved for a wide range of pitching axis locations as long as the pitching stiffness is adequate.

*Corresponding author
Email address: leandro.duarte@icube.unistra.fr (L. Duarte)

Recently, Wang et al. (2017) numerically showed that moving the pitching axis back to the trailing edge can make a fully passive flapping foil turbine to respond in the desired way even for very low flow velocities. A pitching axis located at 35% of the chord length from the leading edge was found to be an optimal condition in their case. Following Wang et al. (2017), Veilleux and Dumas (2017) performed a numerical optimisation for a fixed pitching axis at one third of the chord length and reported hydraulic efficiencies as high as 34%. Subsequently, Boudreau et al. (2018) designed and tested an experimental prototype matching the optimal conditions stated by Veilleux and Dumas (2017) and verified its high performance indicators.

Notwithstanding the significant advances recently achieved in the development of a fully passive flapping foil, its harvesting performance for different pitching axis locations remains unknown. The existence of single frequency large amplitude oscillations has yet to be experimentally observed for a pitching axis located elsewhere than at one third of the chord length.

In an attempt to make up for this shortcoming, a fully passive flapping foil prototype has been designed and tested at the present work. The main objective of this paper is to identify the conditions on the pitching axis location and the pitching stiffness for which an energy harvesting regime can be achieved. A nondimensionalised chart must be provided in order to guide the choice of the adequate pitching stiffness for a given pitching axis location in the design of a fully passive flapping foil hydrokinetic turbine.

This paper is structured as follows: Section 2 provides a preliminary analytical study on the stability of a fully passive flapping foil; Section 3 describes the experimental setup and the procedure for characterising the structural parameters of the prototype; finally, Section 4 presents the experimental protocol, results and discussion.

2. Preliminary analytical study

2.1. Problem modelling

A schematic upper view of a fully passive flapping foil is proposed in Figure 1. It can be modelled by a two degree of freedom mass–spring–damper system, with a heaving motion in the $\vec{y}$ direction and a pitching motion in the $\vec{z}$ direction. The foil interacts with an incompressible fluid flow of specific mass ρ and freestream velocity U_∞ in the $\vec{x}$ direction. On the chord line of the profile, l_θ stands for the distance between the leading edge and the pitching axis location P. The centre of gravity G is considered at a certain distance λ_g from P (positive if P is upstream from G). The chord length is c, while b stands for the span length in the $\vec{z}$ direction. Both heaving position $y(t)$ and pitching angle $\theta(t)$ are taken with respect to an equilibrium position at rest, the chord line being aligned with the flow.

Let m_y, k_y and c_y be respectively the mass, the stiffness and the viscous damping coefficient related to the heaving motion. Analogously, m_θ, k_θ and c_θ will stand

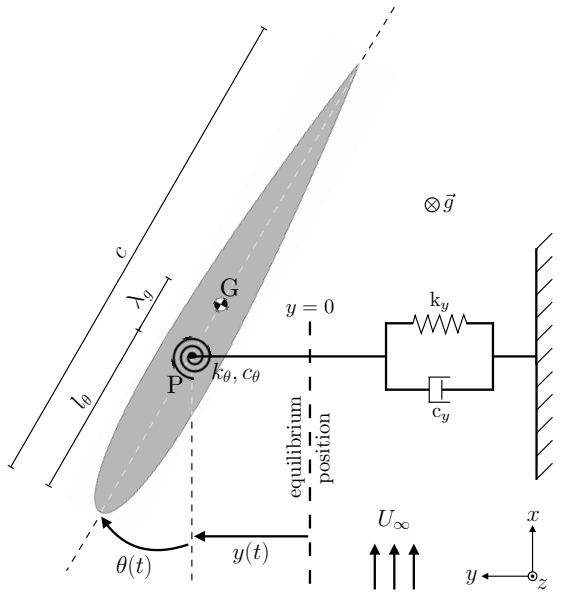

Figure 1: 2D upper view scheme of a fully passive flapping foil hydrokinetic turbine.

respectively for the pitching mass, the rotational stiffness and the viscous damper coefficient related to the pitching motion. The moment of inertia of the foil with respect to the pitching axis at P is I_θ. Finally, kinetic dry friction in both heaving and pitching is considered, respectively, F_K and M_K.

Let F_F be the resultant fluid force over the foil in the plane xy, projected on the heaving axis $\vec{y}$. Let M_F be the fluid pitching moment about the $\vec{z}$ axis at P. Considering a symmetric foil, F_F and M_F are null for an initial condition where the foil rests at the equilibrium position. A slight perturbation of this stable condition leads to non zero fluid resultants, which can cause the foil to move. Applying Newton's second law of motion to the foil, the equations governing its dynamic response in heaving ($\vec{y}$) and pitching ($\vec{z}$) can be written:

$$\begin{cases} m_y\ddot{y} + c_y\dot{y} + k_y y + m_\theta\lambda_g(\dot{\theta}^2\sin\theta - \ddot{\theta}\cos\theta) = F_F - F_K \\ I_\theta\ddot{\theta} + c_\theta\dot{\theta} + k_\theta\theta - m_\theta\lambda_g\left(\ddot{y}\cos\theta\right) = M_F - M_K \end{cases} \tag{1}$$

The parameters involved in the dynamics of the system may be conveniently presented in an nondimensionalised form (taking $*$ as superscript). Assuming the physical quantities of reference $L = c, V = U_\infty, M = \rho bc^2, F = \rho U_\infty^2 bc$, the nondimensionalised parameters are defined in Table 1.

For an energy harvesting regime, the fully passive flapping foil is meant to perform self-sustained oscillatory motions. In order for this to be achieved, the system should have a non-stationary behaviour in the sense that a slight perturbation in the stable initial conditions will cause the foil to diverge from the equilibrium state.

Table 1: Structural parameters of the system with the respective nondimensionalised form.

l_θ	pitching axis location	$l_\theta^* = l_\theta/L$
λ_g	centre of gravity offset	$\lambda_g^* = \lambda_g/L$
m_y	heaving mass	$m_y^* = m_y/M$
k_y	heaving stiffness	$k_y^* = k_y L/F$
c_y	heaving viscous damper	$c_y^* = c_y V/F$
m_θ	pitching mass	$m_\theta^* = m_\theta/M$
k_θ	pitching stiffness	$k_\theta^* = k_\theta/FL$
c_θ	pitching viscous damper	$c_\theta^* = c_\theta V/FL^2$
I_θ	moment of inertia	$I_\theta^* = I_\theta/ML^2$
F_K	heaving kinetic dry friction	$F_K^* = F_K/F$
M_K	pitching kinetic dry friction	$M_K^* = M_K/FL$

2.2. Linear stability analysis

A linear stability analysis is performed as a prior study to the experimental investigations carried out in the following sections. It will enable to reduce the parameter space for the experimental tests by predicting the onset of the non-stationary behaviour of the foil. To do so, Theodorsen's linear reduced model for the fluid resultants is applied (Theodorsen (1935)). Also, it is assumed that the centre of gravity G and the pitching centre P coincide. The non-linear coupling terms related to the static imbalance $\Lambda = m_\theta \lambda_g$ can therefore be neglected. Dry friction in both heaving and pitching is neglected as well.

Under these assumptions, Eqs. 1 can be written in a linearised matrix form:

$$\mathcal{M} \cdot \begin{bmatrix} y & \dot{y} & \ddot{y} & \theta & \dot{\theta} & \ddot{\theta} \end{bmatrix}^\top = 0 \tag{2}$$

with $\mathcal{M}$ a coefficient matrix relying upon the flow and structural properties of the system and the Theodorsen circulation complex function $C(\omega)$ (see Theodorsen (1935)):

$$\mathcal{M} = \begin{bmatrix} A_0 & A_1 & A_2 & A_3 & A_4 & A_5 \\ B_0 & B_1 & B_2 & B_3 & B_4 & B_5 \end{bmatrix}, \tag{3}$$

with:

$$\begin{aligned}
A_0 &= k_y \\
A_1 &= \pi\rho c U_\infty C(\omega) + c_y \\
A_2 &= \pi\rho \left(\frac{c}{2}\right)^2 + m_y \\
A_3 &= \pi\rho c U_\infty^2 C(\omega) \\
A_4 &= \pi\rho \left(\frac{c}{2}\right)^2 U_\infty \left[1 + 2C(\omega)\left(\frac{3}{2} - 2\frac{l_\theta}{c}\right)\right] \\
A_5 &= -2\pi\rho \left(\frac{c}{2}\right)^3 \left(\frac{l_\theta}{c} - 1\right) \\
B_0 &= 0 \\
B_1 &= 2\pi\rho U_\infty \left(\frac{c}{2}\right)^2 C(\omega)\left(2\frac{l_\theta}{c} - \frac{1}{2}\right) \\
B_2 &= \pi\rho \left(\frac{c}{2}\right)^3 \left(2\frac{l_\theta}{c} - \frac{1}{2}\right) \\
B_3 &= 2\pi\rho \left(\frac{c}{2}\right)^2 U_\infty^2 C(\omega)\left(2\frac{l_\theta}{c} - \frac{1}{2}\right) - k_\theta \\
B_4 &= \pi\rho \left(\frac{c}{2}\right)^3 \left[\left(2\frac{l_\theta}{c} - \frac{3}{2}\right) + \right. \\
&\quad \left. 2C(\omega)\left(2\frac{l_\theta}{c} - \frac{1}{2}\right)\left(\frac{3}{2} - 2\frac{l_\theta}{c}\right)\right] - c_\theta \\
B_5 &= -\pi\rho \left(\frac{c}{2}\right)^4 \left[\frac{1}{8} + \left(2\frac{l_\theta}{c} - 1\right)^2\right] - I_\theta
\end{aligned}$$

Applying Laplace transform to Eqs. (2) with zero initial conditions yields a reduced order matrix form:

$$\mathcal{M}_s \cdot \begin{bmatrix} Y_s & \Theta_s \end{bmatrix}^\top = \begin{bmatrix} 0 & 0 \end{bmatrix}^\top \tag{4}$$

with Y_s and Θ_s the Laplace transforms of heaving position and pitching angle, respectively, and $\mathcal{M}_s$ the new coefficient matrix depending on the complex Laplace variable s.

Finding a non-trivial solution of Eq. (4) amounts to solving for the eigenvalues of the matrix $\mathcal{M}_s$. According to the classic control theory stability condition, if one of these eigenvalues has a positive real part the system may have an unstable behaviour. In such a scenario, growing amplitude heaving and pitching motions should emerge out of a slight perturbation in the stable initial conditions.

The main objective of this linear stability analysis is to identify the conditions on the pitching axis location l_θ^* and the pitching stiffness k_θ^* leading to the desired unstable behaviour of the system. To this end, a numerical routine has been implemented to track the eigenvalues of $\mathcal{M}_s$ in the parameter space $l_\theta^* \in [0, 1]$ and $k_\theta^* \in [0, 0.67]$. The stability transition boundary delimiting the stable zone – where all eigenvalues of $\mathcal{M}_s$ have negative real part – to the unstable zone – where there is at least one eigenvalue of $\mathcal{M}_s$ with positive real part – is drawn. First, a baseline simplified case ($c_y^* = 0.75$, $m_y^*, k_y^*, m_\theta^*, I_\theta^*, c_\theta^* = 0$) corresponding to a similar study performed by Peng and Zhu (2009) is considered. Second, the effects of adding inertial properties, pitching damping and heaving stiffness to the system are investigated. The results are illustrated in Figure 2.

Starting with the baseline case, the findings reported by Peng and Zhu (2009) are verified: there is a positive real part eigenvalue of $\mathcal{M}_s$ for $l_\theta^* \geq 0.25$ and k_θ^* sufficiently small. Adding a small quantity of heaving mass to the system does not affect its stability, the transition boundary for $m_y^* < 1.0$ remaining unchanged. If $m_y^* > 1.0$, however, the unstable zone may become larger, as shown in Figure 2.a.

By introducing a non-zero heaving stiffness to a zero mass system, it becomes considerably more unstable: the pitching stiffness needed to stabilise the system for a given $l_\theta^* \geq 0.25$ is increased by a factor of 10. The transition boundary discontinuously jumps to a much higher slope for any $k_y^* > 0$, as can be seen in Figure 2.b. This discontinuity can be explained by the fact that introducing $k_y^* > 0$

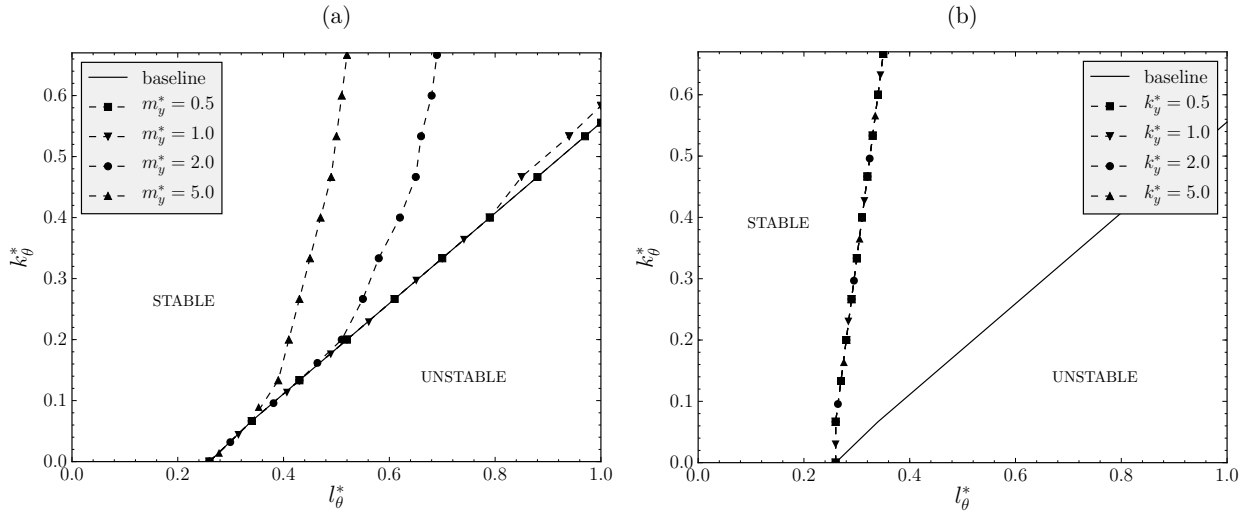

Figure 2: Stability transition boundary of the baseline system ($c_y^* = 0.75, m_y^*, k_y^*, m_\theta^*, I_\theta^*, c_\theta^* = 0$) in the parameter space $l_\theta^* \times k_\theta^*$ depending on (a) the heaving mass m_y^* and (b) the heaving stiffness k_y^*.

causes drastic changes in the matrix $\mathcal{M}_s$, adding a non-zero independent term to its characteristic polynomial. In this case, the system is no more sensitive to the heaving mass. The results did not show any dependency of the stability transition boundary on the moment of inertia I_θ or the pitching damper coefficient c_θ either.

It is important to remember that the stability analysis carried out is applicable only in the vicinity of the equilibrium position. Once the system diverges from it, non-linear events that were not considered in the linear model take place. Particularly, a growing pitching angle can lead to dynamic stall, which may prevent the system from having a chaotic response and make way for limit-cycle oscillations instead. To experimentally investigate the dynamic behaviour of the system from this point, the fully passive flapping foil prototype is presented in next section.

3. Experimental setup

3.1. The technical apparatus

Designed to be tested in a free-surface water channel 0.60 m wide, the flapping foil prototype includes a symmetric NACA0015 profile with a chord length $c = 0.12$ m. Figure 3 provides (a) a schematic front view diagram of the technical apparatus and (b) a picture of the prototype.

With an effective span length $b = 0.50$ m, the foil itself ① is the only part of the prototype that is submerged. It is mounted on a pitching shaft by means of a sliding box ②, allowing for a pitching axis location l_θ^* ranging from 0.20 to 0.60. The pitching shaft is supported by tapered roller bearings inside a shaft casing ③, which is then mounted on the heaving rail through a linear bearing carriage ④. Extension springs ⑤ are used for the heaving stiffness.

The heaving translational motion is converted through a rigid linkage ⑥ into alternative rotational motion of a transmission belt system ⑦, which is linked to an electric servo motor EM_y. The pitching motion is linked to an electric servo motor EM_θ through a transmission belt system ⑧ as well. Heaving position y and velocity $\dot{y}$ are monitored by means of a digital incremental encoder IE_y, while acceleration $\ddot{y}$ is measured with an accelerometer ACC_y. Pitching position θ and velocity $\dot{\theta}$ are also tracked by a digital incremental encoder IE_θ. All these sensors are linked to an I/O FPGA device ⑨, which feeds a closed-loop system controlling the electric currents i_y and i_θ provided to the servo motors. The processing rate is set to 200 Hz, which is about 100 times the flapping foil oscillation frequencies, thus satisfying the Nyquist–Shannon sampling theorem.

It is worth reiterating that this study is focused on investigating the dynamic behaviours of a fully passive flapping foil, i.e. neither heaving nor pitching motions are forced or constrained. The purpose of coupling electric motors to the prototype is to be able to fine-tune the structural parameters of the system. With this setup, one can virtually change the mass, viscous damping, stiffness and dry friction related to the heaving system of certain amounts Δm_y, Δc_y, Δk_y and ΔF_K, respectively. This is done by providing an electric current i_y so that the force F_M applied by the motor EM_y over the heaving system can be written, at an instant t:

$$F_M(t) = \Delta m_y\, \ddot{y}(t) + \Delta c_y\, \dot{y}(t) + \Delta k_y\, y(t) + \Delta F_K\, \mathrm{sgn}[\dot{y}(t)] \tag{5}$$

Analogously, a torque M_M can be provided by the motor EM_θ in order to introduce changes in the viscous damper, stiffness and dry friction related to the pitching system:

$$M_M(t) = \Delta c_\theta\, \dot{\theta}(t) + \Delta k_\theta\, \theta(t) + \Delta M_K\, \mathrm{sgn}[\dot{\theta}(t)] \tag{6}$$

Indeed, adding F_M and M_M to the right-hand side of the equations of motion (Eqs. (1)) produces the desired

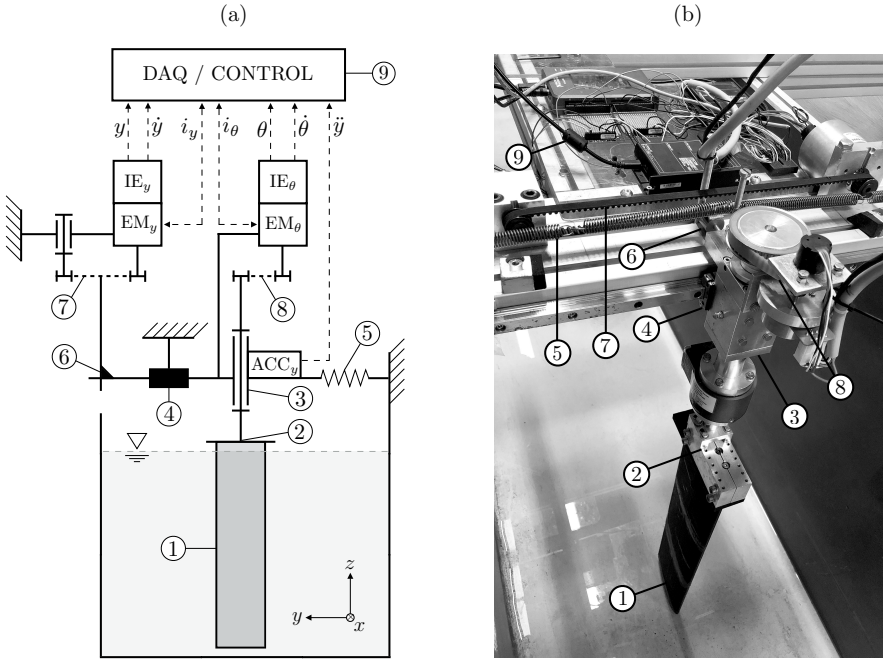

Figure 3: Experimental setup: (a) a schematic front view diagram of the technical apparatus and (b) a picture of the prototype .

effect of virtually changing the structural parameters of the system.

This tuning functionality of the structural parameters is clearly a practical tool for experimentally studying the fully passive flapping foil prototype. A similar force feedback strategy has been developed in the past by Lee et al. (2011) to replace the mechanical damper and springs of the VIVACE harvester (Bernitsas (2008)). In the present study, such technology will be particularly helpful in varying the rotational stiffness k_θ – which will be entirely provided by the servo motor EM$_\theta$ – and in compensating the inherent dry friction on both heaving and pitching motions.

3.2. Characterisation of the structural parameters

The structural parameters of the fully passive flapping foil prototype must be characterised in terms of the model described by Eqs. (1). Among them, the pitching axis location l_θ is directly measured. Stiffness coefficient of the heaving extension springs k_y is characterised in a straightforward manner. Pitching stiffness k_θ is provided by the servo motor EM$_\theta$. Finally, the procedures for determining the inertial and friction properties are described in what follows.

3.2.1. Viscous and dry friction

Starting with the pitching system, a constant torque M_M is applied using the servo motor EM$_\theta$ so that the pitching components, without any stiffness, accelerate from rest. A viscous friction coefficient c_θ and a dry friction torque M_K are considered. Newton's second law of motion leads to a first order linear differential equation for the pitching velocity $\dot{\theta}(t)$, whose analytical solution can be written:

$$\dot{\theta}(t) = \frac{M_M - M_K}{c_\theta}\left(1 - e^{-\frac{c_\theta}{I_\theta}t}\right) \tag{7}$$

with I_θ the moment of inertia with respect to the pitching axis. The system will asymptotically reach a constant angular velocity which is linearly related to the torque M_M applied by the motor:

$$\dot{\theta}_\infty = \frac{1}{c_\theta}M_M - \frac{M_K}{c_\theta} \tag{8}$$

Thus, the viscous friction coefficient c_θ and the dry friction torque M_K are determined by fitting a linear relation to a number of scattered points $(M_M, \dot{\theta}_\infty)$.

With respect to the heaving components, a constant force F_M is analogously applied using the servo motor EM$_y$. The heaving system will accelerate from rest while it crosses the heaving rail. Considering a viscous friction coefficient c_y and dry friction force F_K, the heaving velocity $\dot{y}(t)$ exponentially grows in the same way as in Eq. (7) for the pitching components. It can be written:

$$\dot{y}(t) = \frac{F_M - F_K}{c_y}\left(1 - e^{-\frac{c_y}{m_y}t}\right) \tag{9}$$

with m_y the heaving mass, whose evaluation is described in next subsection. The viscous friction coefficient c_y and the dry friction force F_K are determined by fitting the measured heaving velocity $\dot{y}(t)$ to its transient analytical solution stated by Eq. (9).

3.2.2. Inertial properties

The heaving mass m_y is determined by weighing the heaving parts and adding to it the inertial contribution of the rotating components related to the heaving motion.

The moment of inertia I_θ is evaluated by subjecting the pitching system to an acceleration from rest, just as described in the previous subsection. Supposing c_θ and M_K to be known, I_θ is identified by finding the best fit for the measured pitching velocity $\dot{\theta}(t)$ to its transient analytical solution given by Eq. (7).

Finally, the static imbalance Λ is evaluated by computing the product of the pitching mass m_θ and the distance λ_g, which depends on the pitching axis location l_θ. Let $m_{\theta d}$ be the mass of the pitching components downward from the sliding box, and $x_{\theta d}$ its centre of gravity with respect to the leading edge of the foil. It follows that a linear relationship between the static imbalance Λ and the pitching axis location l_θ can be deduced:

$$\Lambda = m_\theta \lambda_g = m_{\theta d}(x_{\theta d} - l_\theta) \tag{10}$$

The mass of the pitching components m_θ and $m_{\theta d}$ are determined by means of a CAD tool, as well as the centre of gravity $x_{\theta d}$.

4. Results and discussion

4.1. Experimental protocol

All the experiments have been conducted at a chord Reynolds number of 6×10^4, which is achieved by setting the freestream velocity to $U_\infty = 0.5\,\mathrm{m\,s^{-1}}$. A pulse-pair velocity measurement technique (as in Dellinger et al. (2018)) is used to this end.

The characterisation tests revealed that the kinetic dry friction force F_K and moment M_K inherently present in the system are in the same order of magnitude as the fluid forces over the foil. For convenience, those will be henceforth fully counteracted by the electrical motors, allowing for an ideal system without any kinetic dry friction in both degrees of freedom. The pitching viscous friction c_θ is also virtually set to zero. The structural parameters of the experimental prototype baseline case are provided in Table 2 in its nondimensionalised form.

The parameter space of the experimental study consists of varying the pitching axis location l_θ^* in the range of $[0.25, 0.50]$ by increments as fine as 0.015. Values outside that range are of no interest, since the foil remains unconditionally static for $l_\theta^* < 0.25$ – following preliminary results presented in Section 2 – and it is reversed for $l_\theta^* > 0.50$. For each value of l_θ^*, the pitching stiffness k_θ^* is increased by increments of 0.011 until a stationary response is reached. All the other parameters of the system are held constant, unless stated otherwise.

For each test case (l_θ^*, k_θ^*), the foil is released from the equilibrium position at $t < 0$. A slightly perturbation is applied if needed. Heaving position $y(t)$ and pitching angle $\theta(t)$ are then recorded from $t = 0$ during 20 periods of oscillation. Figure 4 provides a picture of the foil from inside de channel during the tests, highlighting y and θ.

Table 2: Baseline nondimensionalised structural parameters of the experimental prototype.

l_θ^*	$[0.250, 0.500] \pm 0.003$
m_y^*	0.50 ± 0.01
c_y^*	0.16 ± 0.03
k_y^*	1.53 ± 0.04
F_K^*	0.00 ± 0.02
I_θ^*	$[0.0187, 0.0217] \pm 0.0016$
c_θ^*	0.000 ± 0.001
k_θ^*	$[0.000, 0.670] \pm 0.008$
M_K^*	0.000 ± 0.001
Λ^*	$[-0.023, 0.026] \pm 0.001$

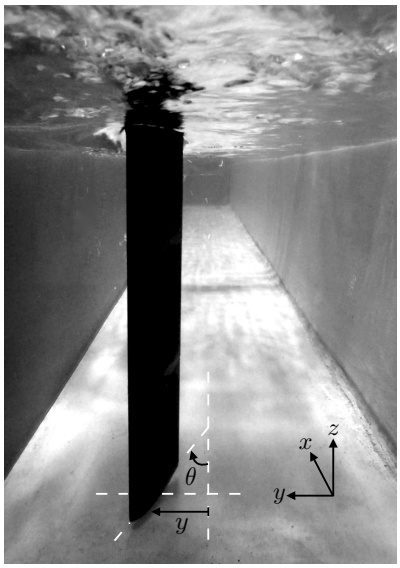

Figure 4: Front picture of the fully passive flapping foil prototype from inside the channel during the tests, highlighting the heaving position y and the pitching angle θ.

4.2. Foil response types

Overall, the same four conceptually different responses found in the numerical study performed by Peng and Zhu (2009) have been observed inside the parameter space studied. Time trace samples of these four different behaviours is provided in Figure 5. A video with the corresponding time traces is provided as well with the online version of this paper.

With the pitching axis located at $l_\theta^* = 0.46$ and a pitching stiffness of $k_\theta^* > 0.46$, it is observed a first stationary behaviour where very low-amplitude oscillations are quickly damped and the foil rests close to the equilibrium position (response I), as shown in Figure 5.a. A second behaviour is identified when reducing the pitching stiffness to $k_\theta^* = 0.12$: the system is no longer static and the foil undergoes high-amplitude periodic pitching and heaving motions around

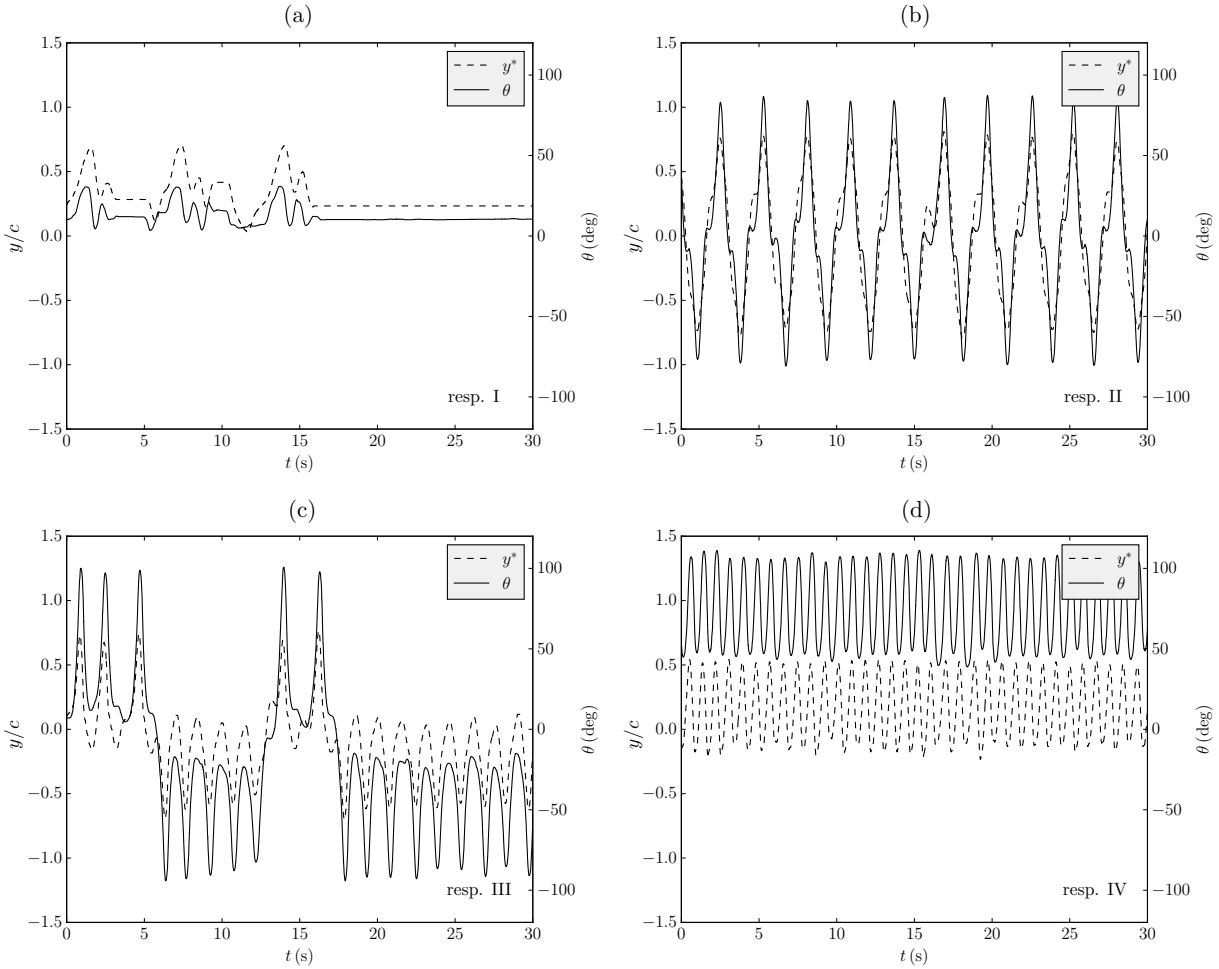

Figure 5: Samples of heaving position y/c and pitching angle θ representing the four different behaviours of the prototype baseline case with $l_\theta^* = 0.46$: (a) response I with $k_\theta^* = 0.46$, (b) response II with $k_\theta^* = 0.12$, (c) response III with $k_\theta^* = 0.06$ and (d) response IV with $k_\theta^* = 0$.

zero (response II), as pictured in Figure 5.b. This is the most attractive behaviour for energy extraction purposes since the heaving amplitude is maximised. Third, reducing further the pitching stiffness to $k_\theta^* = 0.06$ leads to a competition between two stable equilibrium positions disposed symmetrically with respect to zero (response III), just as in Figure 5.c. Finally, setting $k_\theta^* = 0$ keeps the system oscillating about a non-zero pitching angle with no more changing sides (response IV), as can be seen in Figure 5.d. It was also noted that the transitions from the most stable state (response I) to the most unstable one (response IV) are accompanied by an increase in the oscillation frequency of the foil.

The different responses presented in Figure 5 can be qualitatively classified in a straightforward manner. However, a quantitative map would be useful to precisely define the response type even for transitional behaviours, as this would make the classifying process more strict, automatic and robust.

4.3. Classifying map

It is desired to define a classifying quantitative map for the dynamic behaviour of the system in terms of its response type inside the parameter space $l_\theta^* \times k_\theta^*$. This can be done through a scalar function $\mathcal{R} : l_\theta^* \times k_\theta^* \to [0, 1]$ relying upon the time trace of the pitching angle θ. It is conveniently defined:

$$\mathcal{R}(l_\theta^*, k_\theta^*) = 1 - \frac{|\bar{\theta}|}{\theta_{\mathrm{RMS}}} \tag{11}$$

with $\bar{\theta}$ the mean value of the pitching angle and θ_{RMS} its effective value over the recording time T_r for a given test case (l_θ^*, k_θ^*):

$$\bar{\theta} = \frac{1}{T_r} \int_0^{T_r} \theta(t)\, dt \tag{12}$$

$$\theta_{\mathrm{RMS}} = \sqrt{\frac{1}{T_r} \int_0^{T_r} [\theta(t)]^2\, dt} \tag{13}$$

Indeed, in response I the foil remains static with $|\bar{\theta}| \approx \theta_{\mathrm{RMS}}$, which leads to approximate zero values of

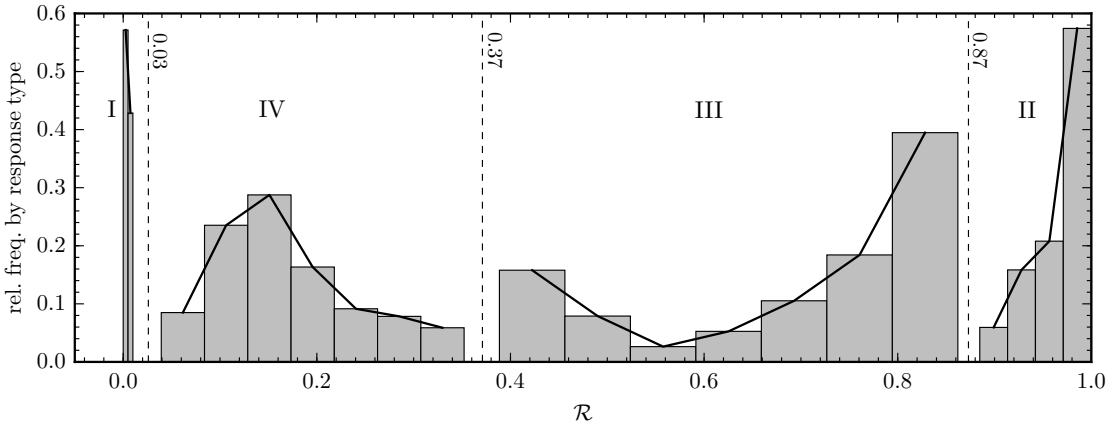

Figure 6: Histogram providing the relative frequency of $\mathcal{R}$ by response type of the prototype observed in the parameter space $l_\theta^* \times k_\theta^*$.

$\mathcal{R}$. Response II is characterised by a nearly zero mean $|\bar{\theta}|$ and a high effective value θ_{RMS}, $\mathcal{R}$ taking values close to 1. The transition between response II and III comes with a slight reduction of the effective pitching angle θ_{RMS} and potentially a decentralisation of the mean value $|\bar{\theta}|$, leading to slightly smaller values of $\mathcal{R}$. Finally, in the transition from response III to response IV, the mean angle $|\bar{\theta}|$ jumps to a considerably higher value, slightly below θ_{RMS}, which leads to small but nonzero values of $\mathcal{R}$.

In order to verify if the response types can be deduced through the function $\mathcal{R}$ without any overlapping, the values of $\mathcal{R}$ for all test cases inside the parameter space $l_\theta^* \times k_\theta^*$ have been computed. The results were then regrouped by response type under a qualitative classifying process. An histogram of the distribution of $\mathcal{R}$ by response type is provided in Figure 6.

An injection between the values of $\mathcal{R}$ and the response types is observed, without any overlapping. It can be stated:

$$\begin{cases} 0 & < \mathcal{R} < & 0.03 & \Rightarrow \text{response I} \\ 0.03 & < \mathcal{R} < & 0.37 & \Rightarrow \text{response IV} \\ 0.37 & < \mathcal{R} < & 0.87 & \Rightarrow \text{response III} \\ 0.87 & < \mathcal{R} < & 1 & \Rightarrow \text{response II} \end{cases} \tag{14}$$

4.4. Response chart

By means of the classifying map $\mathcal{R}$ defined in Eq. (11) and the threshold values stated in Eqs. (14), it is now possible to draw the response chart of the fully passive flapping foil prototype. The contours of $\mathcal{R}$ for all test cases inside the parameter space $l_\theta^* \times k_\theta^*$ are given in Figure 7, delimiting the boundaries between the different responses.

It has been found that the pitching axis must be placed at a distance of at least $l_\theta^* = 0.29$ from the leading edge in order for the foil to present a moving response. In addition, for any $l_\theta^* > 0.29$ there is a critical value of pitching stiffness for which the foil is stationary, delimiting response I. Response II is observed at $k_\theta^* = 0$ for $0.31 < l_\theta^* < 0.39$. Moving the pitching axis further back requires some pitching stiffness in order to keep inside the response II zone, otherwise responses III and IV may arise.

Another interesting finding is that low-amplitude responses III and IV are observed in the transition from response II to I. These transitory responses have not been reported in the numerical simulations of a simplified system by Peng and Zhu (2009).

The experimental results corroborate the previous findings issued from the preliminary linear stability analysis. As shown in Figure 7, the non-stationary behaviour area (responses II, III and IV) is significantly larger than that of a simplified system without any heaving mass or stiffness.

Figure 2.b suggests that, for a pitching axis location of $l_\theta^* = 0.36$, a simplified system should present a stationary behaviour unless $k_\theta^* < 0.08$. At the same pitching axis location, it is experimentally observed a quite larger critical pitching stiffness of about $k_\theta^* = 0.28$, but not as large as the predicted value of $k_\theta^* > 0.67$. This is probably due to the fact that stabilising terms present in the experiments have been neglected in the simplified model. One can cite, in particular, the static dry friction, the outer boundary effects or even the fluid viscosity, which is not fully accounted in Theodorsen's linear model.

4.5. Sensitivity tests

In order to experimentally assess the dependency of the transition boundaries on the heaving mass and stiffness, sensitivity tests were conducted. They consisted of comparing the evolution of $\mathcal{R}$ over vertical trajectories on the parameter space $l_\theta^* \times k_\theta^*$ for different values of m_y^* and k_y^*. The pitching axis locations $l_\theta^* = 0.36$ and $l_\theta^* = 0.46$ are considered. The results are presented in Figure 8.

According to these results, the stability transition boundary from response I to IV does not show any dependence on the heaving mass or stiffness. The critical value of k_θ^* for which $\mathcal{R} < 0.03$ is barely unchanged for a given pitching

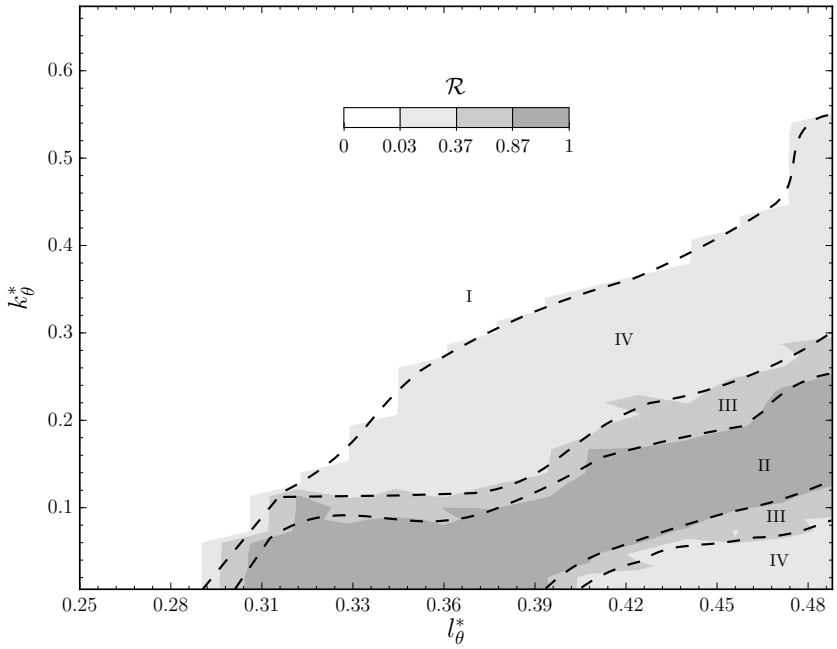

Figure 7: Response chart of the prototype with respect to the pitching axis location l_θ^* and the pitching stiffness k_θ^*, defined by means of the quantity $\mathcal{R} = 1 - |\bar{\theta}|/\theta_{\mathrm{RMS}}$.

axis location. However, the other transition boundaries seem to be slightly dependent on m_y^* and k_y^*.

As a general trend it can be stated that decreasing the heaving mass or increasing the heaving stiffness delays the transitions from response II to response III while crossing the parameter space from $k_y^* = 0$ to $k_y^* = 0.67$. The opposite is also true, the transitions occurring early when increasing the heaving mass or decreasing the heaving stiffness. This suggests that increasing the heaving natural frequency of the prototype may be advantageous for energy harvesting purposes. Indeed, it may keep the system in the response II region for a wider range of pitching stiffness at a given pitching axis location.

5. Conclusion

The dynamic behaviour of a fully passive flapping foil hydrokinetic turbine with respect to the pitching axis location l_θ^* and the pitching stiffness k_θ^* has been experimentally investigated at a Reynolds number of 6×10^4.

Prior to the experimental investigations, a linear stability analysis relying upon Theodorsen's reduced model is performed. The preliminary findings helped defining the parameter space for the experimental study $l_\theta^* \times k_\theta^* = [0.25, 0.50] \times [0.0, 0.67]$. They also provided meaningful insights into the sensitivity of the stability transition boundary to the heaving mass and stiffness.

A fully-passive flapping foil prototype has been designed and tested in a confined channel. Thanks to an original tuning functionality by means of external actuators, the structural parameters of the system could be precisely varied inside the parameter space of the study.

Four conceptually different responses have been experimentally observed. If $l_\theta^* < 0.29$, the foil remains static (response I). Without any pitching stiffness, large amplitude oscillations about the equilibrium position (response II) emerge for $0.31 < l_\theta^* < 0.39$. Moving the pitching axis further towards the trailing edge can make the foil oscillate alternatively around two symmetric non-zero angles (response III), or even oscillate about a single non-zero angle (response IV).

The most suitable behaviour for energy extraction purposes (response II) can be achieved for a wide range of pitching axis location as long as the pitching stiffness is adequate. High values of pitching stiffness tends to stabilise the system. Low-amplitude responses III and IV are observed in the transition from responses II to I.

As a main result, it is provided a nondimensionalised chart with the boundaries between the different responses, which are quantitatively evaluated by means of a scalar function relying on the time traces of the pitching angle. This chart can be useful for knowing the adequate pitching stiffness depending on the pitching axis location in the design of a fully passive flapping foil hydrokinetic turbine.

Finally, the sensitivity of the transition boundaries with respect to the heaving mass and stiffness has been assessed. The tests revealed that increasing the heaving natural frequency of the prototype can enhance its capability of responding in the desired way (response II) for an energy extraction scenario.

Future work must be done in order to evaluate the harvesting performances of the prototype for different pitching axis locations inside response II zone. Moreover, the robustness of the system should be fully assessed in terms of

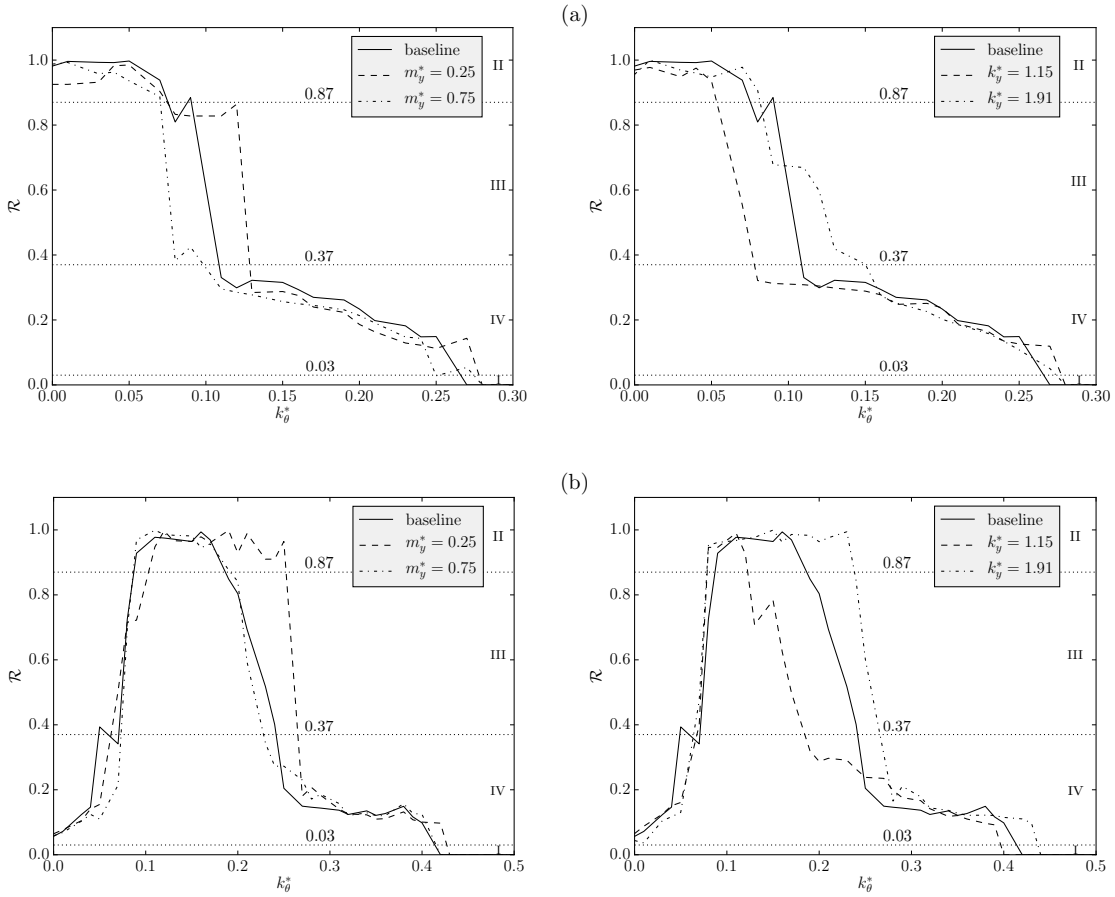

Figure 8: Sensitivity of the transition boundaries between the different responses of the prototype with respect to the heaving mass m_y^* and stiffness k_y^* for a pitching axis location of (a) $l_\theta^* = 0.36$ and (b) $l_\theta^* = 0.46$.

its capability of keeping the desired behaviour under small variations in the flow and structural parameters, including the Reynolds number and the foil geometry.

Acknowledgements

This research project is supported by University of Strasbourg, ICube laboratory and INSA of Strasbourg. The authors would like to show their gratitude to the colleagues from the lab who provided insight and expertise that greatly assisted the research.

References

Bernitsas, M. (2008). Vivace (vortex induced vibration for aquatic clean energy): A new concept in generation of clean and renewable energy from fluid flow. *Journal of Offshore Mechanics and Arctic Engineering*.

Boudreau, M., Dumas, G., Rahimpour, M., and Oshkai, P. (2018). Experimental investigation of the energy extraction by a fully-passive flapping-foil hydrokinetic turbine prototype. *Journal of Fluids and Structures*, 82:446 – 472.

Davids, S. T. (1999). A computational and experimental investigation of a flutter generator. Master's thesis, Naval postgraduate school.

Dellinger, N., François, P., Lefebure, D., Mose, R., and Garambois, P.-A. (2018). An experiment of a hydropower conversion system based on vortex-induced vibrations in a confined channel. *Renewable Energy*, 115:54 – 63.

Kinsey, T. and Dumas, G. (2008). Parametric study of an oscillating airfoil in power extraction regime. *Aiaa Journal - AIAA J*, 46:1318–1330.

Kinsey, T., Dumas, G., Lalande, G., Ruel, J., Méhut, A., Viarouge, P., Lemay, J., and Jean, Y. (2011). Prototype testing of a hydrokinetic turbine based on oscillating hydrofoils. *Renewable Energy*, 36(6):1710 – 1718.

Lee, J., Xiros, N., and Bernitsas, M. (2011). Virtual damper–spring system for viv experiments and hydrokinetic energy conversion. *Ocean Engineering*, 38(5):732 – 747.

Peng, Z. and Zhu, Q. (2009). Energy harvesting through flow-induced oscillations of a foil. *Physics of Fluids*, 21(12):123602.

Theodorsen, T. (1935). General theory of aerodynamic instability and the mechanism of flutter. Technical Report 496, National Advisory Committee for Aeronautics. Langley Aeronautical Lab.; Langley Field, VA, United States.

Veilleux, J.-C. and Dumas, G. (2017). Numerical optimization of a fully-passive flapping-airfoil turbine. *Journal of Fluids and Structures*, 70:102–130.

Wang, Z., Du, L., Zhao, J., and Sun, X. (2017). Structural response and energy extraction of a fully passive flapping foil. *Journal of Fluids and Structures*, 72:96 – 113.

Xiao, Q. and Zhu, Q. (2014). A review on flow energy harvesters based on flapping foils. *Journal of Fluids and Structures*, 46:174–191.

Young, J., Lai, J. C., and Platzer, M. F. (2014). A review of progress and challenges in flapping foil power generation. *Progress in Aerospace Sciences*, 67:2 – 28.

Zhu, Q. (2012). Energy harvesting by a purely passive flapping foil from shear flows. *Journal of Fluids and Structures*, 34:157–169.